



Influence of the Plastic Number on the Evolution of a Yield Stress Material Subjected to a Dam Break

A. V. F. Modolo¹, B. V. Loureiro¹, E. J. Soares¹ and R. L. Thompson^{2†}

¹ *Department of Mechanical Engineering, Federal University of Espírito Santo, Vitória, 29075-910, Brazil*

² *Department of Mechanical Engineering, Federal University of Rio de Janeiro, Rio de Janeiro, Rio de Janeiro 21945-970, Brazil*

† *Corresponding Author Email: rthompson@mecanica.coppe.ufrj.br*

(Received December 21, 2018; accepted February 2, 2019)

ABSTRACT

Dam break problems occur in a variety of applications. In the present paper we are especially concerned with the mining industry, where a dam break can be a catastrophic event with significant harm to the environment. In this case, the materials involved have a yield stress property, i.e., they flow only when a threshold is overcome by the stress that acts on the material. The plastic number, which measures the importance of the yield stress in the overall characteristic stress, is the main dimensionless number analyzed, and carbopol solutions are the kind of material employed. Since slip is common in motions of yield stress materials, the influence of this phenomenon is investigated by a comparison between the flow over a smooth and a rough surface. An image processing that captures the evolution of the shape of the interface as well as particle image velocimetry measurements were employed as tools to understand the role played by the plastic number in the problem. A number of cases presented a triangular depression that originated from a difference between the flow below the initial yield surface position and a rigid body motion above the initial surface position.

Keywords: Yield stress material; Free surface flow; Gravity flow.

1. INTRODUCTION

Gravity current flows are important in many situations covering natural problems like snow avalanches and debris flows, as well as human activities, like unfortunate incidents that happen unexpectedly in mining. In November of 2015, the most harmful environmental disaster in the history of Brazil happened because of a dam break. The consequences of this dam break were the contamination of an important river in the states of Minas Gerais and Espírito Santo by mining waste, interrupting the life of many species as well as the economic activity of local people who depended on the health of the river for their work. A very similar dam break occur again in January of 2019, in the same region, again as a consequence of the mining industry exploration. A review of some of the harmful consequences from dam failures around the world can be found in [Azam and Li \(2010\)](#). Typically, the materials involved in such incidents can be classified as yield stress fluids, since they require a non-zero stress intensity in order to cause motion.

General dam break flows have been studied since the pioneering work of [Ritter \(1892\)](#), but [Dressler \(1954\)](#)

made a more systematic experimental study using boundary layer theory to interpret the results. An advance in the measurement of the front evolution was made with the aid of CCD cameras as studied by [Stansby *et al.* \(1998\)](#) with water as the main fluid. In a similar fashion, [Fraccarollo and Capart \(2002\)](#) investigated the erosion originating from the water invasion of a container with solid particles. Other aspects of the problem were explored by [Miller and Chaudhry \(1989\)](#), who analyzed curved channels, [Bellos *et al.* \(1992\)](#), investigating converging and diverging channels, [Kocaman and Ozmen Cagatay \(2012\)](#), analyzing the effect of lateral channel contraction, and [Soares-Frazaõ and Zech \(2007\)](#), verifying the influence of the presence of obstacles.

Dam break flows of yield stress materials have received some attention in the literature. [Balmforth *et al.* \(2006\)](#) experimentally studied the dam break problem of yield stress fluids and compared the evolution of the interface with the results of a shallow fluid model coupled with the Herschel-Bulkley viscosity model, with limited success. They also re-reported difficulties in reproducing the experiment in a roughened channel. In the context of steep down-ward flumes, [Ancy and Cochard \(2009\)](#) compared a numerical approach employing the

Herschel–Bulkley viscosity model with experimental results, with a quite good agreement. In a subsequent paper, [Cochar and Ancey \(2009\)](#) investigated the spreading dynamics of a yield stress material on an inclined plane with a sophisticated apparatus for image acquisition and processing. [Bates and Ancey \(2017\)](#) analyzed the dam break flow of yield stress fluids in a context where erosion is taken into account.

Although yield stress materials are complex, exhibiting a variety of mechanical responses, the role played by the yield stress, i.e., the viscoplastic nature of this kind of material, still needs to be analyzed in the context of dam breaks. In particular, to isolate the effect of the yield stress from other effects can be a challenging task, depending on how the equations of motion are made dimensionless. The objective of the present paper is to measure the influence of the plastic number on the evolution in time of a viscoplastic material subjected to a dam break condition.

2. EXPERIMENTAL PROCEDURE

2.1 Dimensionless Numbers

The dimensionless numbers that govern the dam break problem are the Froude number (Fr), the Reynolds number (Re), and the plastic number (Pl). The Froude number is usually defined as

$$Fr = \frac{U_c}{\sqrt{gL_c}}. \quad (1)$$

The general expression for the plastic number is $Pl = \tau_y / \tau_s$ ([Thompson and Soares, 2016](#)), where τ_s is a characteristic (shear) stress taken as a supremum value for the shear stress, τ . For problems where an *a priori* characteristic velocity, U_c , is defined, τ_s can be expressed by $\tau_s = \tau(U_c)$. Therefore, in the case of a Herschel–Bulkley model, which will be used to fit the flow curve data, Pl is given by

$$Pl = \frac{\tau_y}{\tau_s} = \frac{\tau_y}{\tau_y + K(U_c / L_c)^n}. \quad (2)$$

In the literature on non-Newtonian fluid mechanics, there is no consensus about the definition of the Reynolds number, as discussed by [Thompson and Soares \(2016\)](#). In fact, there is no consensus even for Newtonian flows in non-circular ducts, as explored by [Costalonga *et al.* \(2018\)](#). Generalizing the expression for Re adopted for ducts by [Kfoury *et al.* \(2017\)](#), one can employ the following expression for the Reynolds number:

$$Re = \frac{\rho U_c^2}{\tau_s}. \quad (3)$$

The experimental approach of this problem faces a challenge, namely, how to change one single dimensionless number without affecting the others. The main difficulty is to change either the Froude or the Reynolds number, maintaining the other fixed for

different materials. This problem comes from the fact that the characteristic velocity affects the three numbers (Fr , Re , Pl). While Re and Pl depend directly on material properties, this is not so for the Froude number, making a dimensionless analysis almost impossible. In other words, one has to choose between maintaining the Reynolds or the Froude number fixed. The traditional approach, in problems where gravity is the main cause of motion, is to select Fr as the dimensionless number to be controlled. Therefore, in order to compare the different viscoplastic materials employed, we keep the same Froude number for each case and vary the plastic number in order to capture the influence of this parameter, which is the essential dimensionless quantity associated to the material. The problem analyzed in the present paper does not have an *a priori* characteristic velocity, but has a characteristic stress given by $\tau_c = \rho g H_0$, where H_0 is the height of the level of the fluid before the motion starts, chosen to be the characteristic length of the problem. We adopted as characteristic velocity the inertial one [Huilgol and Kefayati \(2015\)](#), i.e., the velocity that arises from the balance of inertial stress with the characteristic stress, which means that $U_c = \sqrt{2gH_0}$. In this approach, the Froude number is fixed and its value is $Fr = \sqrt{2}$.

2.2 Setup

The experimental setup was based on the aspect ratios adopted by [Carrivick *et al.* \(2011\)](#). The aquarium was made in plexiglass, which enables visualizing the flow and acquiring images during the tests. The height of the aquarium is 303 mm and its thickness was 50 mm. The reservoir where the liquid was contained was 400 mm in length while the empty space to which the fluid advances was 1092 mm long. Other details about the aquarium are displayed in Fig. 1. Initially the fluid remains at rest in the reservoir, separated from the rest of the domain by a gate also made of plexiglass. Before the gate was abruptly opened, the image acquisition was started with a CCD camera or the PIV apparatus, depending on the case.

The tests were performed both with Newtonian and yield stress fluids. In the latter case, in order to test the influence of wall slip, sandpaper was added to the bottom of the aquarium and a comparison was made with the smooth case (no sandpaper).

2.3 CCD Camera Technique and Image Capturing

The work station employed in the image capturing procedure is composed of the equipment described as follows. An analog monochromatic camera with progressive sweep, brand MANTA G-201C, with 2 megapixel of resolution, sensor Sony ICX274 CCD, and maximum resolution of 14.7 frames per second. The CCD camera was employed for the Newtonian and yield stress fluids, which in the present case are transparent. In order to improve the image acquisition, a low concentration black dye was added to the working fluid. The camera is located at a distance of 2.1 m from the setup in order to capture

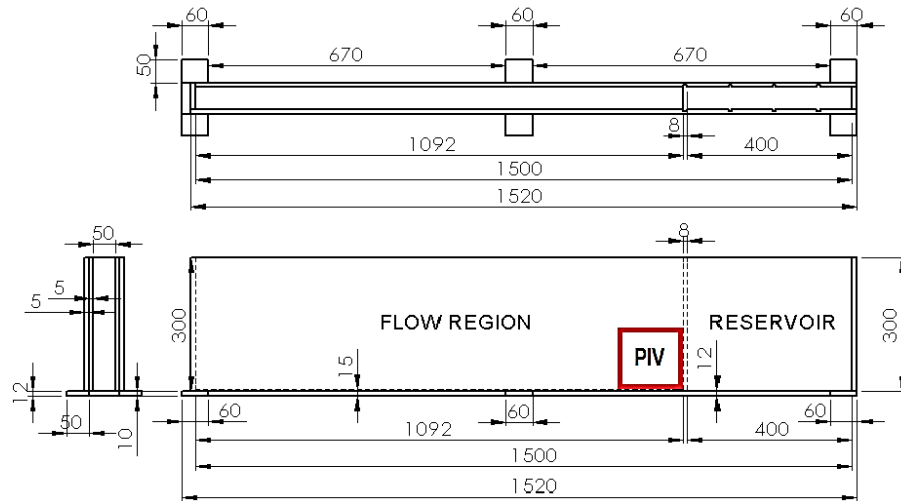


Fig. 1. Scheme of the setup.

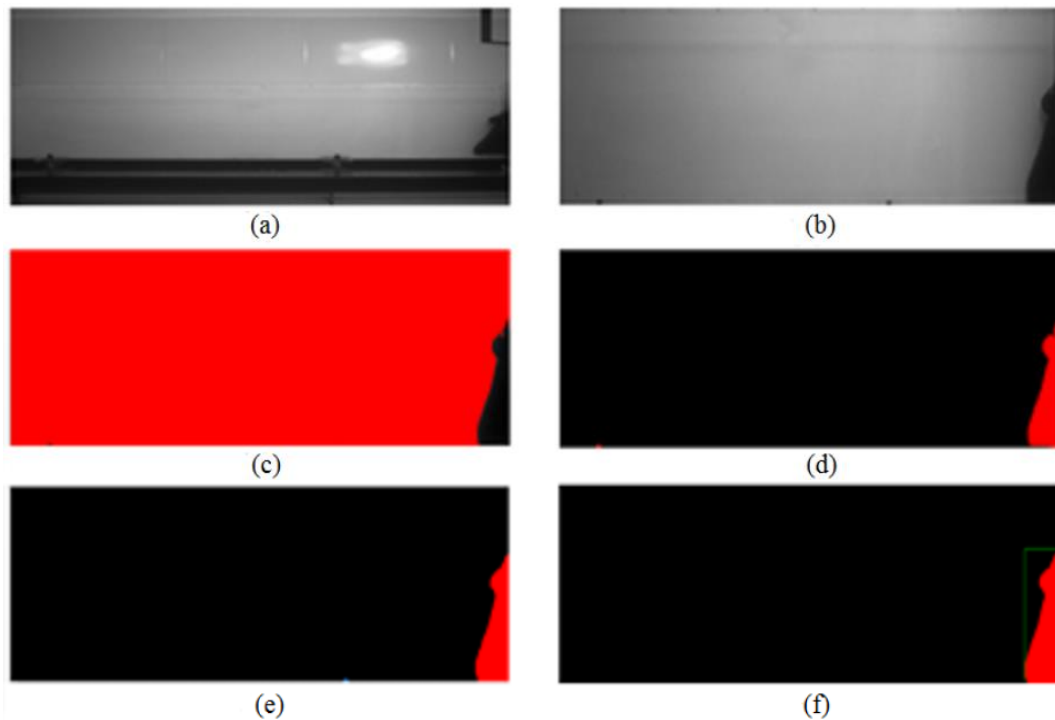


Fig. 2. Steps to get a final image from the original image captured by the camera.

the complete domain of the flow. The image processing was executed with an algorithm developed by Vision Assistance 7.1 from National Instruments.

A typical image processing is shown in Fig. 2. The image processing stages are: (a) Original image; (b) Selection of the image area to be processed; (c) Identification of the air-fluid interface; (d) Conversion of the image to 8 bits; (e) Adjustment of the morphology and the elimination of spurious particles; (f) Frame the flow domain.

2.4 Particle Image Velocimetry Technique

The tracer particles employed are glass spheres of the

kind SEED PARTICLES-GLSS-HLLW with a mean diameter varying between $8 \mu\text{m}$ and $12 \mu\text{m}$. A double-pulse Nd: YAG laser was used in the PIV measurements. In addition, a CCD camera, a synchronizer, and a computer equipped with the software INSIGHT 4G-2DTR were needed to complete the whole system for data acquisition and processing. All this equipment is from TSI Incorporated. After the acquisition of a pair of images, they are calibrated in order to map pixels into real values. The processing stage consists in dividing the first image into 64×64 -pixel interrogation windows and analyzing where the groups of particles of the first window are in the second one. The second image is swept using the

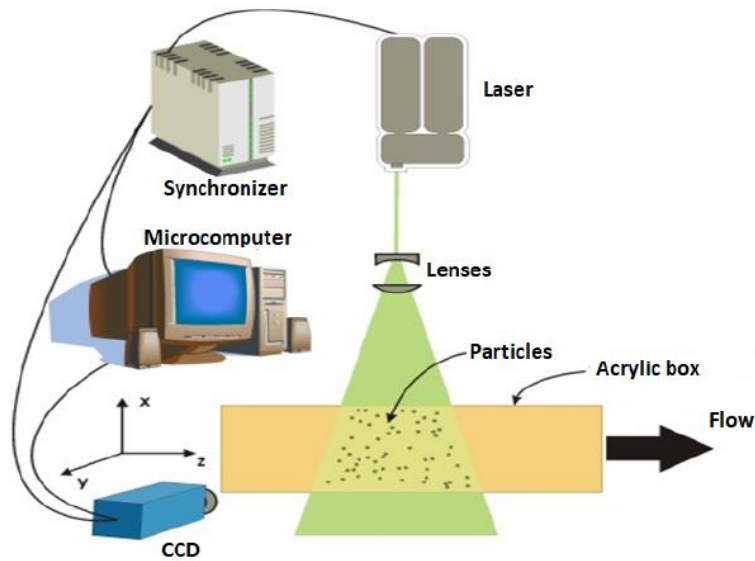


Fig. 3. Scheme of the PIV measurements.

same dimensions as the first one and the new position is obtained from the cross correlation functions. The software performs a post-processing in order to eliminate spurious velocity vectors, which are eventually computed by the probabilistic technique employed in the cross correlation, and replacing this vector by an interpolated one. The PIV tests were conducted in a similar manner to the ones with the CCD camera. The total test time was smaller, since the PIV analysis was performed in a smaller domain (165 mm × 125 mm), illustrated in Fig. 1 as a red rectangle.

2.5 Materials Employed and Rheometry

The viscoplastic materials employed were solutions of *Carbopol* 980 in water. The different concentrations of these solutions were 1.5%, 1%, 0.75%, 0.5% and 0.25%. For the preparation of the solutions, the carbopol powder was added to water and stirred with an angular velocity of 1200 rpm in a stirrer with a capacity of 15 liters. After 30 minutes of intense stirring, the solution was kept at rest for 22 hours. After this stage, a solution of 18% NaOH in water was added, while the stirring rate was kept at 300 rpm. The stirring of the complete solution was maintained for more than two hours. This procedure was employed in order to guarantee a stable and homogeneous solution.

The experiments for the rheological characterization of the carbopol solutions were conducted in a commercial stress controlled rheometer HAAKE MARS II, by ThermoScientific. This apparatus can provide reliable measurements above a minimum torque of 5.10 Nm. The selected geometry was the cross-hatched parallel plates with a diameter of 35 mm in order to avoid slipping at the wall, as highly recommended by the literature.

Figure 4 shows the flow curves obtained from the rheometric measurements of the carbopol solutions for the concentrations employed. The concentrations

of 0.25% and 1% were repeated with different samples. The 1% carbopol solutions exhibited very similar flow curves, while the cases where the concentration was 0.25% showed a little discrepancy.

The Herschel–Bulkley equation, $\tau = \tau_y + K\dot{\gamma}^n$, was used to fit the experimental measurements and to estimate the rheological features, such as the yield stress. The curve fittings, represented by full lines, extrapolates the experimental points and allows one to identify the yield stress fitting values. As expected, the yield stress increased with the concentration of carbopol. Their corresponding values are: $\tau_y^{0.25\%} = 65.5$ Pa, $\tau_y^{0.5\%} = 88.6$ Pa,

$$\tau_y^{0.75\%} = 101.4$$
 Pa, $\tau_y^{1.0\%} = 108.1$ Pa, and

$$\tau_y^{1.5\%} = 115.8$$
 Pa. The exponent index of the model

does not vary too much from one case to another, having an approximate value of $n \approx 0.3$.

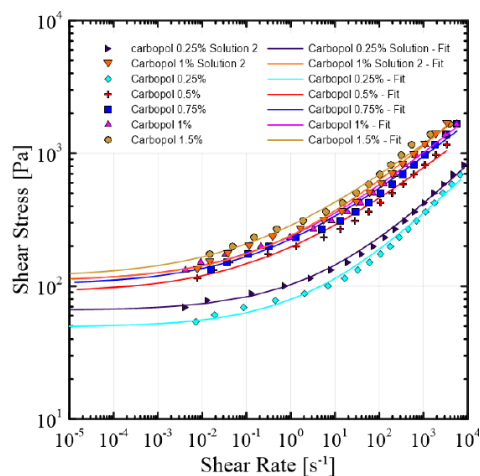


Fig. 4. Flow curves of the different carbopol solutions.

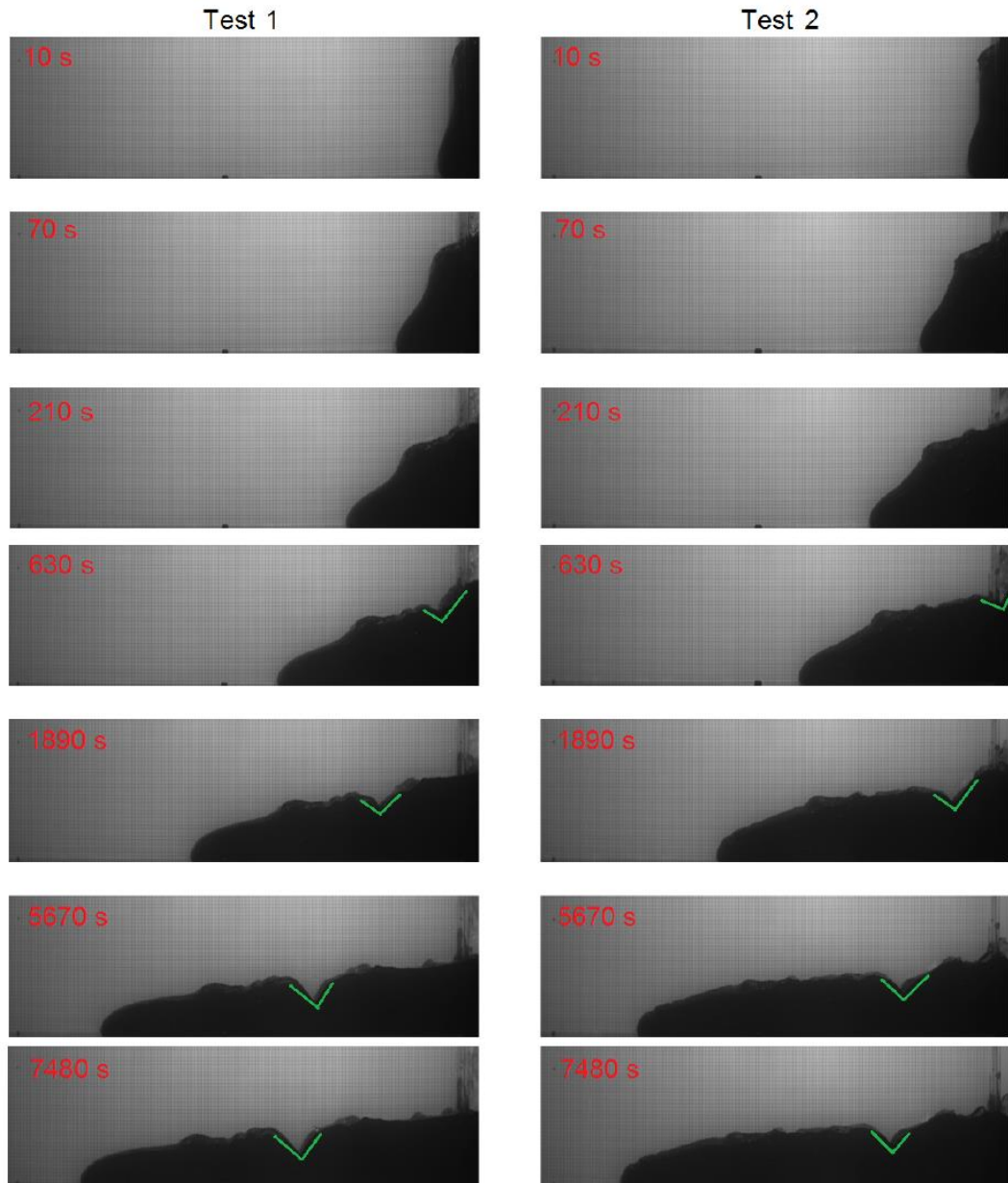


Fig. 5. Image as captured by the camera of two different samples of a 1% carbopol solution. Each sample corresponds to a column. At the top left of each subfigure, in red, is registered the elapsed time in seconds from the beginning of the experiment.

3. RESULTS

Before showing the results we obtained in the Dam Break problem, we would like to register that, for each solution, it was conducted two runs and that the difference between the two runs can be a measure of the uncertainty associated to the problem at the specific solution. Some of these results are displayed in Figs. 5, 10 and 11

3.1 Images Captured

Figure 5 shows some images captured by the technique described previously for solutions of 1% weight of carbopol in water. It can be noticed that the evolution of the yield stress material can be

clearly identified, since there is a color contrast between the material domain and the surroundings. The images of the right column were captured at the same elapsed time as the corresponding ones in the left column. This experiment was performed in order to provide an idea of the reproducibility of the problem: from the preparation of the material until the evolution itself. As can be seen, the repeatability is quite good, since the results of the two tests are very similar to each other.

In Fig. 6 it is shown the final stage where the evolution of each carbopol solution has stopped. In this figure, we can see in more detail how the material is distributed. First of all, we notice an irregular shape, typical of yield stress materials

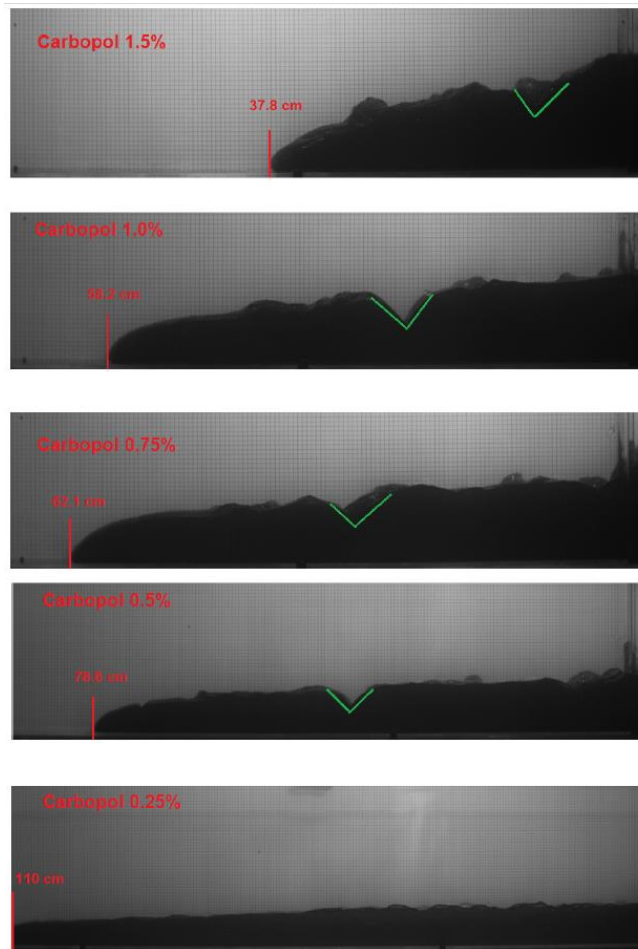


Fig. 6. Image as captured by the camera of the different carbopol solutions tested at the final time $t = 7480s$ where no motion is detected in any solution.

Ancey and Cochard (2009). This irregularity is tri-dimensional and is more accentuated for higher concentrations of carbopol. These final images reveal that the final shape of these materials forms an inclined interface, which is expected for yield stress materials. While a difference in height in a Newtonian fluid induces a stress that the fluid cannot resist, in a material with viscoplastic properties, the stress induced by differences in height has to overcome the yield stress in order to lead to motion.

Therefore, a difference in height can be statically sustained. Needless to say, the final inclination is higher for materials with higher values of the yield stress, since the resistance to motion increases with the yield stress and a larger height discrepancy can be supported. Since the volumes are equal, a direct consequence is that higher inclinations lead to lower stopping positions, as shown by the images and as registered in red, with a red bar marking the maximum range reached by the material. The lower concentration carbopol solution did reach the end of the tank.

An interesting fingerprint of the progression of these yield stress materials was the appearance of a kind of more or less triangular depression that travels with the material as it evolves. Green lines are drawn in the figures in order to help the reader to locate these

“triangular depressions.” In some cases, the depression does not extend over the whole cross section area and therefore the green lines contrast with a first glance interpretation. However, this manifestation of the motion occurred in almost every case tested (except for the carbopol solution with the lowest yield stress). We note that this phenomenon can be found with more or less intensity in other yield stress material experiments Ancey and Cochard (2009) but have not been captured by models. The origin of such a depression seems to be associated to a bending that occurs above the yield surface on the material in the first instants after the gate is pulled. This unyielded structured material bends towards the same direction of the motion. Due to the flow conditions, the lower part of the motion acquires a higher velocity and the unyielded portion of the material never tumbles, but forms the depression seen in the images.

A possible explanation for this phenomenon could be associated to the phenomenon of shear-banding. Following Bonn *et al.* (2017) (see Fig. 24 of that paper), shear-banding could be explained by a range of shear rates with the co-existence of two shear stress values associated to a single imposed nominal shear rate. In addition to a dynamic flow curve there exists a static branch, where $\dot{\gamma} = 0$. However, the

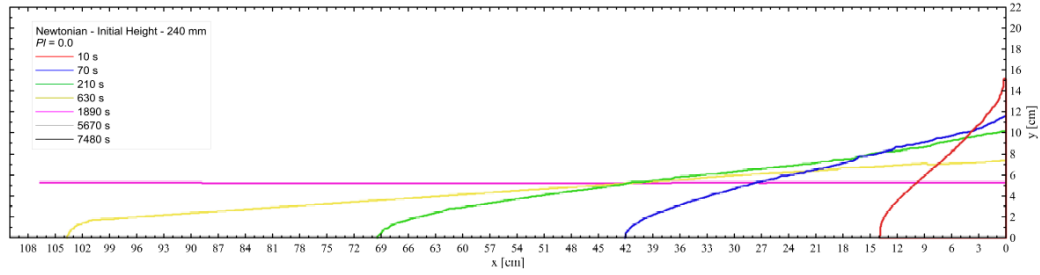


Fig. 7. Evolution of the frontline for the Newtonian fluid. The lines correspond to physical times $t = 10s, 70s, 210s, 630s, 1890s, 5670s,$ and $7480s$.

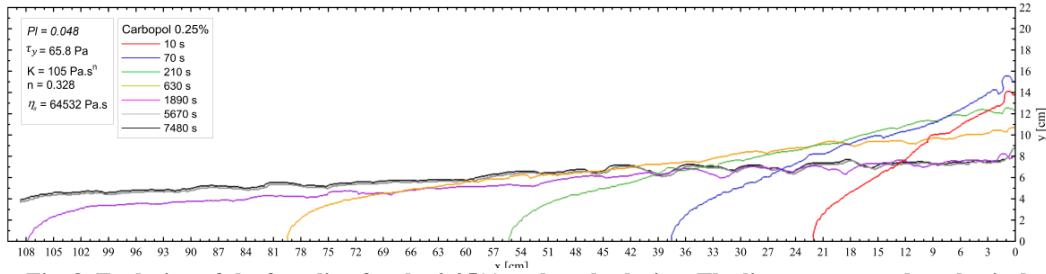


Fig. 8. Evolution of the frontline for the 0.25% carbopol solution. The lines correspond to physical times $t = 10s, 70s, 210s, 630s, 1890s, 5670s, 7480s$.

experiments conducted in the present work are stress-based, in the sense that the stress (and not the motion) is imposed. Therefore, it is expected that the material would follow the static branch before it breaks. It also seems unlikely the flow would retard after breaking down. Since this same rationale applies to non-monotonic flow curves, another reason for this phenomenon must be found. Next, we elaborate another conjecture.

If we assume that the von Mises criterion of yielding is applicable, we can compute the location of the yield surface at the instant t_0 when the gate is taken off, using the following rationale. When the material is totally confined, the vertical compression that the material would experience is contained and an isotropic stress, a pressure, acts on the material. The von Mises criterion takes a quantity that scales with the second invariant of the stress tensor and, therefore, an isotropic stress cannot induce yielding. However, when the gate is pulled, the stress caused by gravity is no longer isotropic because the fluid is not totally confined anymore. Therefore, the fluid experiences a compression with a stress, induced by gravity, τ_G , such that $\nabla \cdot \tau_G = -\rho g \mathbf{e}_y$, where y is the vertical coordinate, ρ is its mass density, and g is the acceleration due to gravity. This gravity stress is given by

$$\tau_G = \rho g (H_0 - y) \mathbf{e}_y \mathbf{e}_y \quad (4)$$

where $\mathbf{e}_y \mathbf{e}_y$ is the normal dyadic associated with the

y direction. The von Mises stress is $\tau_{vM} = \sqrt{\frac{1}{2} \tau_G^{dev,2}}$

, where τ_G^{dev} is the deviatoric part of τ_G . At the

beginning of motion, $\tau_{vM} = \frac{\sqrt{3}}{3} \rho g (H_0 - y)$. In

order to find the von Mises yield surface, y_c , we have to put the von Mises stress equal to the yield stress, i.e.,

$$\tau_{vM}(y = y_c) = \frac{\sqrt{3}}{3} (H_0 - y_c) = \tau_y \Leftrightarrow y_c = H_0 - \frac{\sqrt{3} \tau_y}{\rho g} \quad (5)$$

This rationale gives a rough location of the yield surface, which can vary between ≈ 1.1 cm to ≈ 2 cm below the maximum height of the problem, depending on the value of the yield stress. This value is compatible with the problem with a initial height of $H_0 = 24$ cm.

3.2 Evolution of the Frontline

In this subsection, we present the evolution of the frontline for the different materials employed in this study. As a reference for comparison, the Newtonian case is shown in Fig. 7. The initial height is fixed at $H_0 = 24$ cm for all cases. From Fig. 7 to 18, each plotted line corresponds to a fixed elapsed time from the beginning. A general comparison between the Newtonian case and the viscoplastic ones is that the very flat surfaces obtained in the Newtonian case are replaced by roughness surfaces between the viscoplastic material and the air, as already pointed out. Another fact worth noticing is that the absence of a yield stress in the Newtonian fluid leads to an evolution that ends with a horizontal line interface.

The mapping of an image like the ones presented in Figs. 5 and 6 is a 2-D representation of a 3-D surface and, therefore, needs a filtering. In the present case this is done by the simple projection of the 3-D surface on the neutral plane.

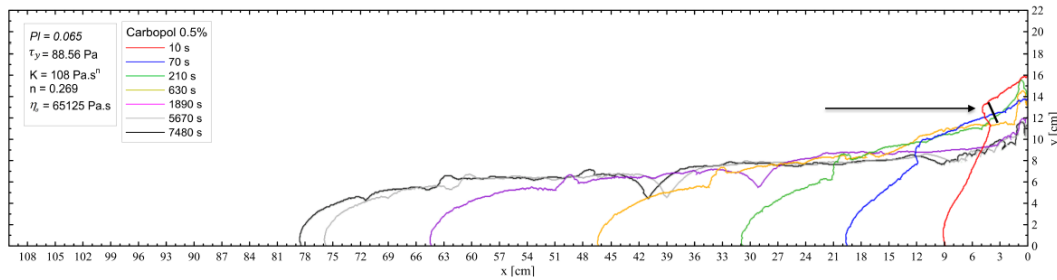


Fig. 9. Evolution of the frontline for the 0.5% carbopol solution. The lines correspond to physical times $t = 10\text{s}, 70\text{s}, 210\text{s}, 630\text{s}, 1890\text{s}, 5670\text{s}, 7480\text{s}$.

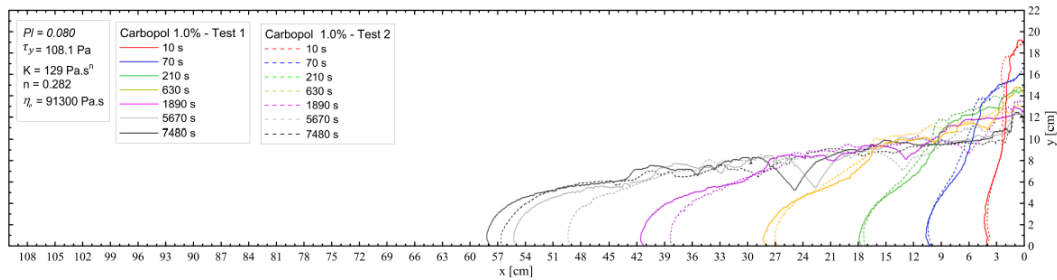


Fig. 10. Evolution of the frontline for the 1.0% carbopol solution. Two tests were performed in order to verify repeatability. The lines correspond to physical times $t = 10\text{s}, 70\text{s}, 210\text{s}, 630\text{s}, 1890\text{s}, 5670\text{s}, 7480\text{s}$.

A comparison of Figs. 7 and 8 shows that the addition of 0.25% in weight of carbopol in water significantly changes the evolution of the material after the gate is quickly opened. The Newtonian fluid rapidly achieves its final horizontal configuration, filling the bottom part of the tank uniformly. A fact worth noticing is the shape of the advancing fluid. In the case of a yield stress material, the detachment from the line that describes a linear interface in the majority of the domain comes earlier, leading to a more fingering shape near the bottom, when compared to the Newtonian case, where this linearity has a much higher range.

In Fig. 9, where the evolution of a 0.5% carbopol solution is shown, we notice a much slower motion than the one developed by 0.25% carbopol solution. This evolution clearly shows that the phenomenological origin of the “triangular” depression that repeatedly occurred in a number of cases is due to a bending of the unyielded material that is above the original yield surface. The red shape of the yield stress evolution at $t = 10\text{ s}$ reveals the beginning of this process. A black bar pointed by a black arrow indicates the size of the unyielded portion of the material that starts to bend. From the marks in the right coordinate, we notice that the rationale developed previously, where this size can be approximated by $\sqrt{3}\tau_y / (\rho g)$, provides a reasonable estimate for the length found in the figure. Following the interface at the successive instants $t = 70\text{ s}$ (blue line) and $t = 210\text{ s}$ (green line), we are able to verify how the depression, which is easier to identify at $t = 630\text{ s}$ (purple line), is formed.

The cases of the higher concentrations of 1.0% and 1.5% carbopol are shown in Figs. 10 and 11, respectively. In these cases, we also exhibit a

comparison of the two tests. The evolution of the front line provides a better representation of the analysis than the examination of the images of Fig. 5. The color code is maintained in the same fashion as the previous results. Test 1 is represented by full lines while Test 2 is shown in dotted lines. In the case of the 1.0% carbopol solution, Fig. 10, we notice that at $t = 10\text{ s}$ there is a negligible difference in the bottom part of the material. The upper part presents some little discrepancies. At $t = 70\text{ s}$, these discrepancies dislocate to the center portion of the material but, at $t = 210\text{ s}$, they reach the triple point (yield stress material, air, solid surface). The difference between the position of the advancing triple points corresponding to Test 1 and Test 2 enlarges as time progresses to $t = 630\text{ s}$, $t = 1890\text{ s}$, and $t = 5670\text{ s}$. However, comparing the final position reached in each test, we notice only a small relative discrepancy. This happens because, as discussed previously, the final inclination is mainly a function of the yield stress, which is the same for the two cases. Therefore, any difference that can occur during the transient motion is mitigated as the motion comes close to its end and the material achieves its final configuration. In the case of the 1.5% carbopol solutions, Fig. 11, we observe that, at $t = 10\text{ s}$, the discrepancy between the configurations of Test 1 and Test 2 is a little bit higher than in the 1.0% carbopol solution. However, they do not spread in the subsequent evaluated times. Again, both triple points are closer at the final stage.

Figure 12 shows the percentage difference, ξ , between the advancing triple point of a carbopol solution and the corresponding value of the Newtonian triple point at the same time. This quantity is computed by

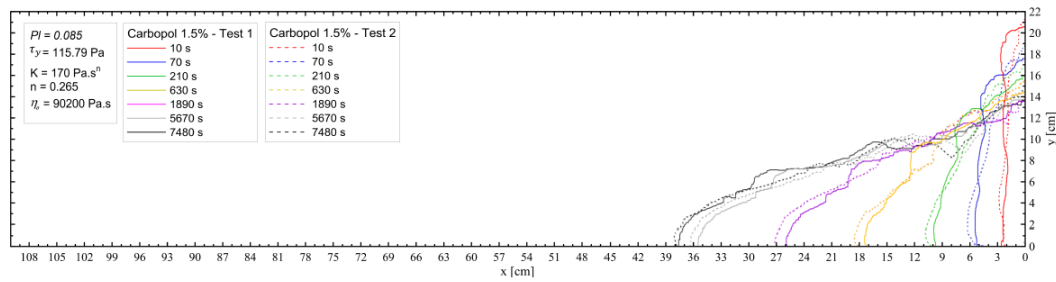


Fig. 11. Evolution of the frontline for the 1.5% carbopol solution. Two tests were performed in order to verify the repeatability. The lines correspond to physical times $t = 10s, 70s, 210s, 630s, 1890s, 5670s, 7480s$.

$$\xi = 100 \frac{x_r - x_s}{x_r}, \quad (6)$$

where x_s is the position of the solution and x_r is the triple point position of the reference triple point, in this case the 0.25% carbopol solution. We can see that there is a minimum at $t \approx 300$ where ξ is a minimum for all cases. For higher plastic numbers, this tendency is accentuated, i.e., there are higher slope values for the descending and ascending regions.

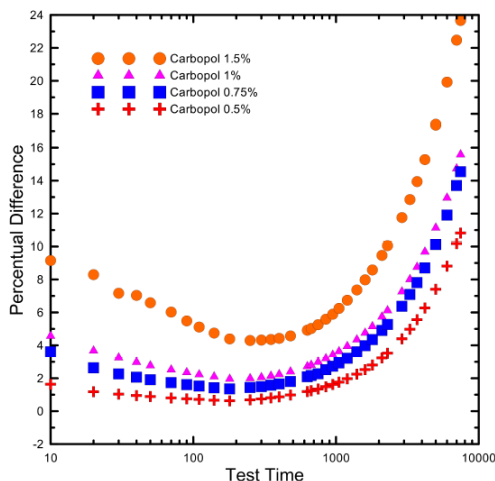


Fig. 12. Relative evolution of the frontline for the different carbopol solutions employed, as represented by the percentage difference of the front position of the solution with respect to the least plastic case (0.25% carbopol solution).

3.3 Slip at the Bottom Wall

Slipping is a concern in yield stress materials. In order to verify the existence of slip effects at the bottom wall, we glued sandpaper to this surface of the tank. It is known that in the laminar regime a roughness like this is not able to induce a significant extra drag. Figures 13 and 14 show the PIV results comparing the evolution of these materials with and without the sandpaper during the first stages of motion for two solutions of carbopol, 0.25% and 1%, respectively. The color code goes from blue to red, from the lowest to the highest velocity. Even in very

early stages of the motion ($t = 28$ s), Figs. 13(a) and 13(b) reveal that the velocities of the 0.25% carbopol solution are higher, even with the overall shape of the two evolutions being more or less the same at this instant. When time evolves to $t = 68.4$ s, Figs. 13(c) and 13(d) show that the case with no sandpaper has advanced more than the case with sandpaper. It is worth noticing that the bluish region associated to very low velocities is thicker in the motion with the presence of the sandpaper and is near the triple contact point (solid, yield stress material, and air).

This tendency continues in the subsequent stage captured in Figs. 13(e) and 13(f) ($t = 206.4$ s). We can observe that the sandpaper has accelerated the appearance of a nub of material associated to different reactions of the yielded and unyielded parts of the material. In the case of the 1% carbopol solution, Fig. 14, again the velocities associated to the sandpaper case are lower. In this case, we notice a more uniform advance of the yield stress material in the smooth case. A similar nub also disturbs the inclination plane of the material, but in the case of the 1% carbopol solution the sandpaper has retarded its appearance. At time $t = 68.4$, the smooth case has its higher velocities concentrated at the nose of the advancing front and there is a large portion of the material that, even though being in contact with the solid surface, does not present a bluish region. At this same instant, the motion for the sandpaper case shows a distribution of high velocities more aligned to the inclination of the free surface. Figs. 15 and 16 show comparisons between the cases with and without the sandpaper motions, (full and dotted lines, respectively), for the same pair of materials. The cases for the 0.25% carbopol solution, presented in Fig. 15, have frontline shapes that coincide very much at $t = 10$ s. The distance between both triple points gradually increases as time elapses. A similar effect occurs for the 1% carbopol solution, observed in Fig. 16. In this second case, it seems that the sandpaper has imposed a more restrictive condition, making the more concentrated solution stop at an earlier stage. Hence, slippage is more likely to occur in materials with higher yield stress. In order to provide a more direct comparison between the slipping effect experienced by the two materials, we show the evolution of the relative position of the triple point for both fluids in Fig. 18. This percentage difference, ξ , is computed by Eq. (6), but now, the reference is the position of the case with sandpaper.

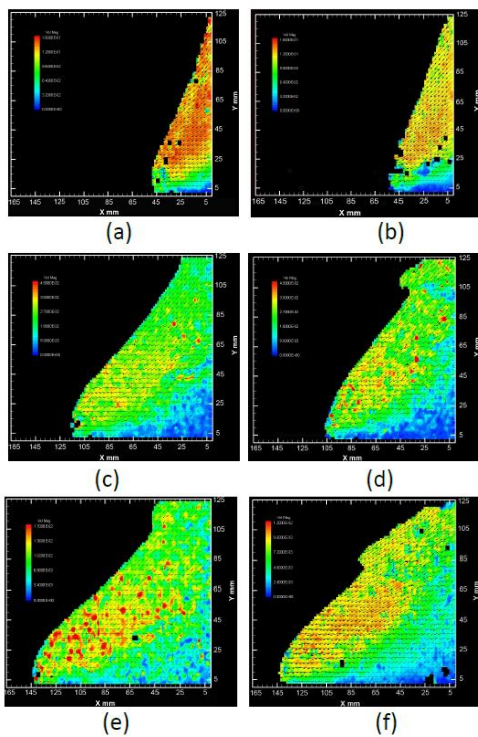


Fig. 13. Comparison of the frontline evolution of the 0.25% carbopol solution between the smooth and rough bottom wall surfaces.

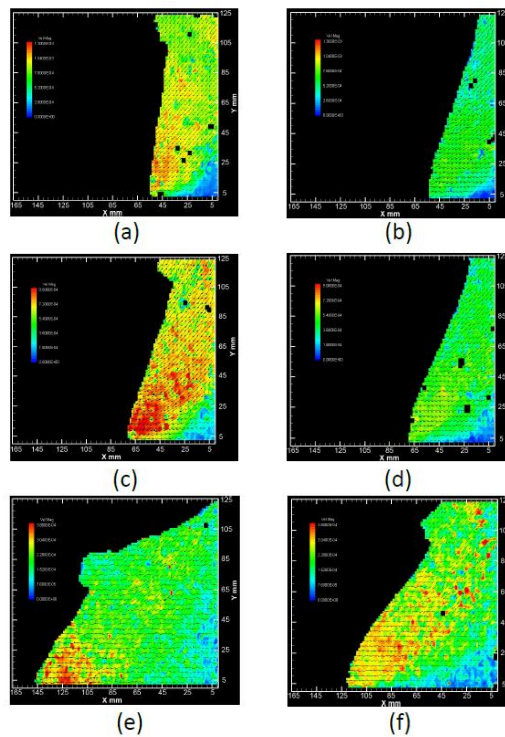


Fig. 14. Comparison of the frontline evolution of the 1.0% carbopol solution between the smooth and rough bottom wall surfaces.

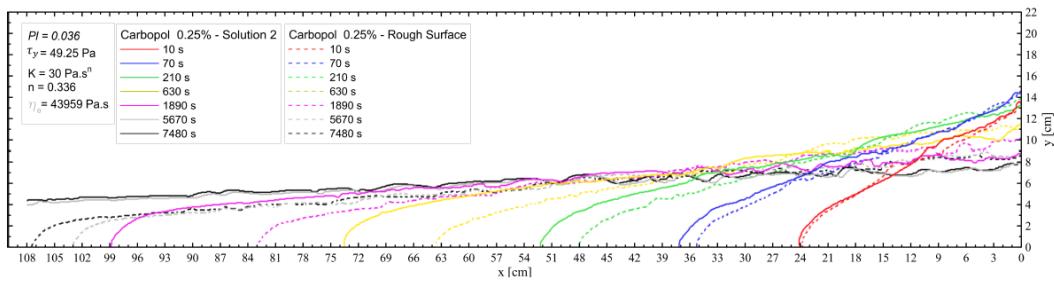


Fig. 15. Comparison of the frontline evolution of the 0.25% carbopol solution between the smooth and rough bottom wall surfaces.

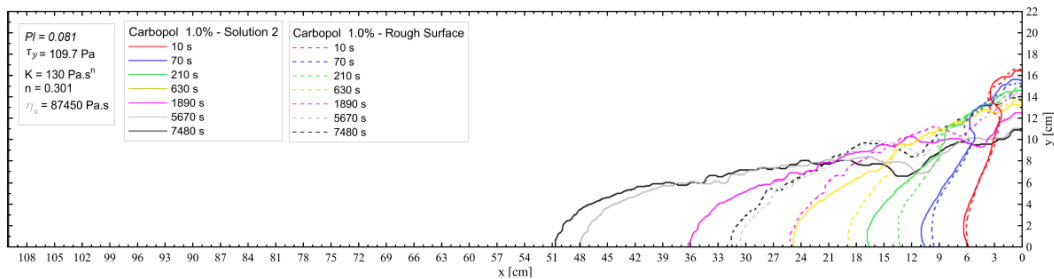


Fig. 16. Comparison of the frontline evolution of the 1.0% carbopol solution between the smooth and rough bottom wall surfaces.

While the 0.25% carbopol solution exhibited an expansion and a retraction of the percentage difference between the cases with and without the

sand-paper, the yield stress material with 1% carbopol solution showed a monotonic increase of ξ .

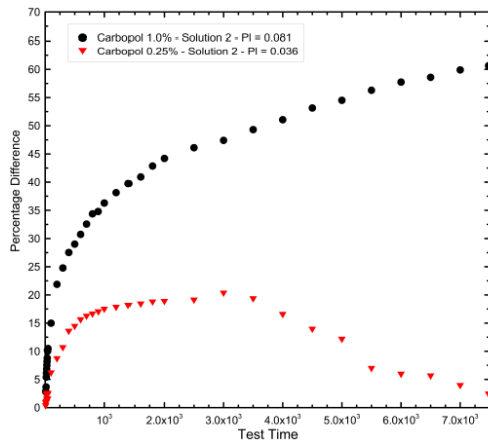


Fig. 17. Percentage difference between the frontline evolutions with respect to the rough and smooth surfaces for the 0.25% and 1.0% carbopol solutions.

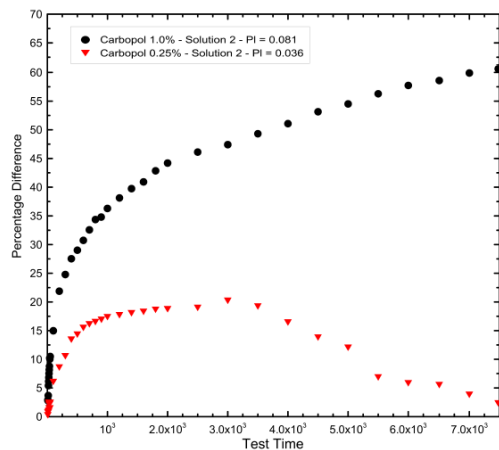


Fig. 18. Percentage difference between the frontline evolutions with respect to the rough and smooth surfaces for the 0.25% and 1.0% carbopol solutions.

4. CONCLUSION

We performed a Dam Break experiment with carbopol solutions of several concentrations which corresponded to different plastic numbers, while the Froude number was maintained. The image capturing and processing and the PIV measurements allowed tracking the motion and analyzing some aspects of the velocity field during the first stages of motion. We were able to attest the repeatability of the problem from the rheological and motion perspectives to within a small tolerance. The shape of the free surface between the material and the air was irregular. Generally, a nub (of material) or a more pronounced triangular depression (with no material) was formed and advected by the flow. We could show that this phenomenon is associated to the position of the yield surface before motion starts, determined by the total height and the yield stress of the material. The tests with the yield stress materials revealed that the end of motion preserves an inclination of the surface in contact with the air,

associated to the presence of a yield stress. In order to evaluate the influence of the slip at this boundary, sandpaper was glued to the bottom of the tank and the motion was compared to the case without sandpaper. The PIV results have shown that there is some slip at this wall, by measuring a non-vanishing velocity in the case without the sandpaper. The percentage difference of the position of the advancing front, ξ , was computed for two values of the plastic number. While the case with a lower plastic number showed an increase and decrease of ξ over the course of the trajectory, the case with the higher plastic number exhibited a monotonic increase of this parameter.

ACKNOWLEDGMENTS

This research was partially funded by grants from CAPES (Brazilian Graduate Education Foundation) and CNPq (Brazilian Research Foundation).

REFERENCES

- Ancey, C. and S. Cochard (2009). The dam-break problem for herschel–bulkley viscoplastic fluids down steep flumes. *Journal of Non-Newtonian Fluid Mechanics* 158, 18–35.
- Azam, S. and Q. Li (2010). Tailings dam failures: a review of the last one hundred years. *Geotech News* 28(4), 50–54.
- Balmforth, N. J., R. V. Craster, P. Perona, A. C. Rust and R. Sassi (2006). Viscoplastic dam breaks and the bostwick consistometer. *Journal of Non-Newtonian Fluid Mechanics* 142, 63–78.
- Bates, B. M. and C. Ancey (2017). The dam-break problem for eroding viscoplastic fluids. *Journal of Non-Newtonian Fluid Mechanics* 243, 64–78.
- Bellos, C. V., J. V. Soulis and J. G. Sakkas (1992). Experimental investigation of two dimensional dam-break induced flows. *Journal of Hydraulic Research* 30, 47–63.
- Bonn, D., M. M. Denn, L. Berthier, T. Divoux and S. Manneville (2017). Yield stress materials in soft condensed matter. *Reviews of Modern Physics* 89(035005), 1–40.
- Cochard, S. and C. Ancey (2009). Experimental investigation of the spreading of viscoplastic fluids on inclined planes. *Journal of Non-Newtonian Fluid Mechanics* 158, 73–84.
- Costalonga, M. L., B. V. Loureiro and E. J. Soares (2018). Drag reducing flows by polymer solutions in annular spaces. *Journal of Fluids Engineering* 140(051101), 1–8.
- Dressler, R. F. (1954). Comparison of theories and experiments for the hydraulic dam break wave. *International Association of Scientific Hydrology* 38, 319–328.
- Fraccarollo, L. and H. Capart (2002). Riemann wave description of erosional dam-break flows.

- Journal of Fluid Mechanics* 461, 183–228.
- Huilgol, R. R. and G. H. R. Kefayati (2015). Natural convection problem in a bingham fluid using the operator-splitting method. *Journal of Non-Newtonian Fluid Mechanics* 220, 22–32.
- Kfourri, S. L. D., E. J. Soares, R. L. Thompson and R. N. Siqueira (2017). Friction losses for power-law and viscoplastic materials in abrupt contractions and expansions. *Journal of Fluids Engineering* 139(021203), 1–16.
- Kocaman, S. and H. Ozmen-Cagatay (2012). The effect of lateral channel contraction on dam break flows: Laboratory experiment. *Journal of Hydrology* 432–433, 145–153.
- Miller, S. and M. H. Chaudhry (1989). Dam-break flows in curved channel. *Journal of Hydraulic Engineering* 115, 1465–1478.
- Ritter, A. (1892). The reproduction of the aquatic waves. *Journal Association of German Engineers* 36, 947–954.
- Soares-Frazão, S. and Y. Zech (2007). Experimental study of dam-break flow against an isolated obstacle. *Journal of Hydraulic Research* 45, 27–36.
- Stansby, P. K., A. Chegini and T. C. D. Barnes (1998). The initial stages of dam-break flow. *Journal of Fluid Mechanics* 374, 407–424.
- Thompson, R. L. and E. J. Soares (2016). Viscoplastic dimensionless numbers. *Journal of Non-Newtonian Fluid Mechanics* 238, 57–64.